Isotope effects in electron-impact dissociation of D2H+

P Defrance, J J Jureta, J Lecointre, X Urbain

Isotope effects in electron-impact dissociation of D_2H^+

P. Defrance[1], J. J. Jureta[1, 2], J. Lecointre[1] and X. Urbain[1]

[1]Université Catholique de Louvain, Institute of Condensed Matter and Nanosciences, Chemin du Cyclotron 2, B-1348 Louvain-la-Neuve, Belgium

[2]Institute of Physics, University of Belgrade, P.O.Box 68, 11081, Belgrade, Serbia

Abstract

Absolute cross sections have been measured using the crossed electron–ion beams method for electron-impact dissociation of the D_2H^+ molecular ion yielding H^+, D^+, HD^+ and D_2^+ fragments. The collision energy ranges from a few eV up to 2.5 keV. Around the maximum, cross sections are found to be of similar amplitude: $(3.25\pm0.08)\times10^{-17}$ cm^2 for H^+, $(3.56\pm0.15)\times10^{-17}$ cm^2 for HD^+ and $(3.33\pm0.11)\times10^{-17}$ cm^2 for D_2^+; except for D^+ for which the maximum cross section is $(4.62\pm0.09)\times10^{-17}$ cm^2. Individual contributions for dissociative excitation and for dissociative ionization are determined for each product. Close analysis of present data brings into evidence isotope effects in the fragmentation pattern of the D_2H^+ target. Ejection of the lightest isotope is generally favored: for resonant dissociative excitation (H^+ over D^+), for dissociative excitation (molecular ions D_2^+ and HD^+, associated with ejection of H and D, respectively) and for dissociative ionization, but not for H^+ and D^+ produced via dissociative excitation. Present dissociative excitation cross sections for D_2H^+ are found to be significantly lower than those measured for D_3^+, although those of DI agree well together.

PACS: 34-80, 52-20

Key words: deuterium, hydrogen, isotope, molecular ion, electron–ion collision, ionization, excitation, dissociation, cross section.

1. Introduction

Dissociation of small polyatomic ions is an important process in the chemistry of planetary atmospheres, interstellar clouds [1] and various laboratory experiments [2]. Many deuterated molecules have been detected in the interstellar environment where the material is mainly in the molecular form. The observation of deuterated molecules appears to be easier than that of atomic deuterium itself. The cosmic ratio [HD]/[H_2] is detected to be in the order of 10^{-5},

which coincides with the expected value of the elemental [D]/[H] ratio [3]. Polyatomic deuterated molecules are enhanced in deuterium in comparison to their hydrogenated counterparts and the isomeric ratio [XD]/[XH] is found to be around 10^{-2}. In warm interstellar regions, such the Orion bar, the cosmic ratio $[H_2D^+]/[H_3^+]$ is observed to be 0.02. In cold dense regions, where gas-phase species are expected to accrete on dust grains, chemical fractionation occurs so HD efficiently reacts with H_3^+ to form H_2D^+, D_2H^+ and D_3^+ [4]. Studies of interstellar chemistry including all isotopologues of H_3^+ predict that, in dense depleted regions, the abundance of H_2D^+ is similar to that of D_2H^+ and they also predict that D_3^+ is abundant [5].

Breakup dynamics and the isotope effect in the dissociation of H_3^+ and of D_3^+ have been theoretically studied by Strasser et al [6]. Because of the $\boldsymbol{D}_{3h}$ symmetry, a small isotope effect is likely to be due to the difference in the width of the initial wave function for these two isotopologues. For H_2D^+ and for D_2H^+, the $\boldsymbol{D}_{3h}$ symmetry is broken and only the $\boldsymbol{C}_{2v}$ symmetry remains. Based on the Born-Oppenheimer approximation, the potential energy surfaces of these heteronuclear targets (H_2D^+ and D_2H^+) are identical to that of the homonuclear targets (H_3^+ and D_3^+). Rotational excitation of H_2D^+ and of D_2H^+ is lower than that of symmetric species because asymmetric isotopologues exhibit a non-vanishing permanent dipole moment (unlike H_3^+ and D_3^+), so they can radiatively cool down and reduce both vibrational and rotational internal energies [7].

The experimental results of Strasser et al [7] give evidence for an enhanced occurrence of linear dissociation geometries in the dissociative recombination (DR) of H_2D^+ and of D_2H^+, revealing isotope effects. For H_2D^+, the D atom dominantly lies between the two hydrogen atoms (H–D–H), while no preference for the linear H–H–D (or D–H–H) geometry is observed. The situation is reversed for D_2H^+, in which case the linear D–D–H (or H–D–D) geometry is preferred compared to the linear D–H–D configuration. The force driving the breakup causes a larger acceleration when acting on the H atom than on the D atom. It influences the dissociation process by favoring the ejection of the lighter fragment. Weak enhancements of symmetric dissociation geometries were also found for H_3^+ and D_3^+ [6], but results were difficult to analyze because the three constituents are indistinguishable.

In the DR of H_2D^+, the relative fraction of the two two-body channels (H_2+D and HD+H) is constant over the whole energy range [8]. However, in the DR of D_2H^+, Buhr et al [9] have recently found that the two-body (D_2+H and HD+D) relative fraction is constant up

to 0.2 eV but it strongly changes in the 1–10 eV energy range. The relative fraction $2(D_2+H)/(HD+D)$ is expected to be 1 in the absence of any isotope effect, but it is measured to be 1.27±0.05 at relative electron–ion energies around 0 eV and it is found to increase to 3.7±0.5 at about 5 eV. This large isotope effect implies that, in the DR of D_2H^+, the formation of D_2+H is more favorable than that of HD+D. It appears that the general tendency in DR reactions is to favor ejection of the lightest fragments and to fractionate into the heaviest deuterated molecules.

Buhr et al [9] estimated the population distributions of the vibrational levels for the molecular fragments $D_2(v)$ and $HD(v)$. They were found to be similar for both channels and similar to the distributions obtained in the DR of H_3^+ and D_3^+ [6]. The deduced vibrational populations are wide, showing a bell-shape-like behavior (centered on v= 5–7) covering all possible vibrational states up to v= 15 or even v= 20. For D_2H^+, only the vibrational states within the electronic ground state of the fragments are energetically accessible in both channels: the available final states are $D_2(X^1\Sigma_g(v))$+H(1s) with v= 0 to 20 and $HD(X^1\Sigma_g(v))$+D(1s) with v= 0 to 17, respectively. The shape of the distribution is independent of the isotope and the shift in the position of the most populated quantum state reflects the different vibrational level spacing of the species. In contrast to homonuclear H_3^+ and D_3^+, the heteronuclear D_2H^+ should have lower internal excitation because the latter possesses an electrical dipole moment, allowing a much faster radiative decay of the rotational excitation. Diatomic fragments formed in electronically excited states are not expected to remain bound because of strong predissociation and because of radiative decay to the $^3\Sigma_u$ dissociative state. The decay of excited singlet and triplet states tends hence to contribute to three-body fragmentation.

Electron-impact experiments on deuterated molecular ions are currently performed in our laboratory by means of a crossed electron–ion beams set-up. Absolute cross sections and kinetic-energy-release distributions have been published for dissociation of the homonuclear D_3^+ target [10]. Results have been reported for formation of D^+ and D_2^+ ions, from their respective appearance thresholds up to 2.5 keV. For both fragments, an overall good agreement is observed in the energy region below 30 eV between our results and those of storage ring facilities measured by Jensen et al [11] and by Le Padellec et al [12]. Appearance energies are measured to be (4.5±0.5) eV and (6.0±0.5) eV for D^+ and for D_2^+ respectively. For D^+, the cross section displays a broad peak in the low electron energy range, which is attributed to resonant dissociative excitation (RDE). The threshold measured at (14.0±1.0) eV

is in good agreement with the vertical excitation energy calculated for direct dissociative excitation [13]. For D_2^+, no isolated RDE peak can be clearly observed and the non-zero cross section below the direct DE threshold reflects the width of the Franck-Condon region of the D_3^+ ground state. Dissociative excitation cross sections (σ_{DE}) as well as dissociative ionization cross sections (σ_{DI}) have been separately obtained for both fragments. Dissociative ionization thresholds are observed at (11.0±0.5) eV and at (12.0±0.5) eV, for D^+ and D_2^+ production, respectively. Both thresholds are observed to be analogous, around 11.5 eV, which is too low to be consistent with a Franck-Condon transition. A shoulder is discernible in the cross section at about 30 eV and it is expected to correspond to the energy threshold of the DI process because it is close to the vertical ionization threshold of H_3^+ (33.47 eV).

In order to obtain a more comprehensive understanding of the isotope effect on electron–ion collisions in the hydrogen family, we present here the experimental study of the electron-impact dissociation of the isotopologue D_2H^+. Results are reported for the production of the H^+, D^+, HD^+ and D_2^+ fragment ions. Dissociation of this heteronuclear molecular target proceeds via ten possible reaction channels:

$$D_2H^+ + e^- \rightarrow H^+ + D_2 + e^- \quad (1)$$
$$\rightarrow H^+ + D + D + e^- \quad (2)$$
$$\rightarrow D^+ + HD + e^- \quad (3)$$
$$\rightarrow D^+ + D + H + e^- \quad (4)$$
$$\rightarrow HD^+ + D + e^- \quad (5)$$
$$\rightarrow D_2^+ + H + e^- \quad (6)$$
$$D_2H^+ + e^- \rightarrow HD^+ + D^+ + 2e^- \quad (7)$$
$$\rightarrow H^+ + D_2^+ + 2e^- \quad (8)$$
$$\rightarrow H^+ + D^+ + D + 2e^- \quad (9)$$
$$\rightarrow D^+ + D^+ + H + 2e^- \quad (10)$$

Dissociative excitation (DE) processes are represented by reactions (1–6) and the dissociative ionization (DI) ones by reactions (7–10). In the present experiment, individual ionic fragments result from both DE and DI reactions. A specific procedure has been developed to separate the contributions and absolute cross sections are reported separately for DE and for DI, from their respective thresholds up to 2.5 keV [14].

2. Experimental method and apparatus

The animated crossed electron–ion beams method is applied [15]. The molecular ion beam of well-defined energy (a few keV) interacts at right angles with the electron beam whose energy is tuned from a few electron volts up to 2.5 keV. Product ions are separated from the primary ion beam by using a double focusing 90° magnetic analyzer. Product ions are further deflected by a 90° electrostatic spherical deflector and directed onto the channeltron detector [10].

The electron beam is swept across the ion beam in a linear motion at a constant speed u. The total number of events K produced during one complete electron beam movement is related to the measured cross section σ_m by

$$\sigma_m = \frac{uK}{I_e I_i \gamma} \frac{v_e v_i q_i e^2}{(v_e^2 + v_i^2)^{1/2}} \tag{11}$$

In this expression, γ is the detector efficiency, I_e and I_i, e and $q_i e$, v_e and v_i, are the electron and ion beam current intensities, the charges and velocities of electrons and ions, respectively. Assuming $m_i >> m_e$, the interaction energy E (eV) is given by:

$$E = V_e + \frac{m_e}{m_i}\left(q_i V_i - V_e\right) \tag{12}$$

where V_e and V_i, m_e and m_i are the acceleration voltages and masses of electrons and target ions, respectively.

Due to the transfer of internal potential energy, dissociation fragments exhibit both broad velocity and broad angular distribution in the laboratory frame. The angular acceptance of the magnet analyzer allows the total transmission of the angular distribution of product fragments emitted at a given velocity v in the laboratory frame. In order to put the cross section on absolute scale, the velocity distribution is computed and the total cross section σ is obtained by integrating this distribution over the entire velocity range.

The sum of the kinetic energy released to the dissociation fragments is represented by E_{KER}. By assuming the fragmentation of the target to be binary only and by applying the momentum conservation, this sum is given by

$$E_{KER} = \frac{m^2 w^2}{2\mu} \tag{13}$$

where w represents the fragment speed in the centre of mass frame. Ionic products basically form two velocity distributions whose shapes depend on the various E_{KERs} involved. At low energies, only DE is observed and the spectrum is narrow, which corresponds to low E_{KERs}.

Above the ionization threshold, the spectrum becomes broader because of the Coulomb repulsion experienced by DI fragments. For the H^+, D^+, HD^+ and D_2^+ fragments, the mean kinetic energies are measured to be 4.2, 4.7, 4.1 and 2.9 eV and 9.2, 6.4, 8.6 and 8.3 eV, for DE and for DI, respectively. The maximum corresponding uncertainty is of ±10%. The DI signal is isolated by fitting the broader part of the spectrum. Absolute values of DE cross sections σ_{DE} are obtained by subtracting the DI contribution σ_{DI} from the total absolute cross section σ for each fragment [14]. To help visualize dissociative contributions, corresponding cross sections are reproduced using linear combinations of the analytic expressions which are based upon a Bethe-Born form:

$$\sigma(E) = a \times \left(1 - \frac{E_{th}}{E}\right)^b \times \left(\frac{1}{E}\right) \times \ln\left(e + c \times E\right) \qquad (14)$$

where e is Euler's constant, a, b and c are fitting parameters and E_{th} is the threshold energy.

The total uncertainty (90% confidence limit) for the absolute cross sections is estimated to be about 10%, at maximum, and that associated to the electron energy is estimated to be ±0.5 eV [14].

3. Results and discussion

Absolute total cross sections for the production of H^+, D^+, HD^+ and D_2^+ are grouped in figure 1 (for clarity reasons, error bars are not systematically shown in this figure). Around the maximum, the cross sections for H^+, HD^+ and D_2^+ are found to be of similar amplitude, whereas the maximum cross section for D^+ is found to be larger. The maximum total cross sections are measured to be $(3.25\pm0.08)\times10^{-17}$ cm^2 for H^+, $(3.56\pm0.15)\times10^{-17}$ cm^2 for HD^+, $(3.33\pm0.11)\times10^{-17}$ cm^2 for D_2^+ and $(4.62\pm0.09)\times10^{-17}$ cm^2 for D^+. In figures 2(a–d), absolute total cross sections are presented individually for H^+, D^+, HD^+ and D_2^+, respectively, together with their respective DE contributions while the DI contributions are presented separately in figure 2(e). Energy thresholds for dissociation of H_3^+ and of D_2H^+ are listed in table 1 and absolute total cross sections are given in table 2, together with the associated total uncertainties. The following cross section ratios are presented in figure 2(f) in order to search for an apparent fingerprint of isotope effects: $2[H^+ + D_2]/[D^+ + HD]$ (DE for atomic ions), $2[D_2^+ + H]/[HD^+ + D]$ (DE for diatomic ions) and $2[D_2^+ + H^+]/[HD^+ + D^+]$ (DI).

Figure 1 and Table 1

3.1. H^+ channel

Figure 2(a) shows the results for the formation of the H^+ fragment together with the DE contribution (H^++D_2, or H^++D+D). The DI contribution attributed to the H^+ channel is that of the D_2^+ fragment ($H^+ + D_2^+ + 2e^-$, reaction (8)). Because of unfavorable signal-to-noise ratio it has not been possible to obtain the DI contribution directly from the H^+ channel. The maximum DE cross section (reaction (1) or (2)) is measured to be $(1.98\pm0.15)\times10^{-17}$ cm^2 at 35 eV, which is close to the maximum DI cross section ($H^+ + D_2^+$) that is found to be $(2.13\pm0.06)\times10^{-17}$ cm^2 at 75 eV. For energies above 50 eV, the DI contribution is observed to be noticeably higher than that of DE.

The H^+ appearance energy at (5.5±0.5) eV fairly agrees with the energy threshold of reaction (1) (H^++H_2+e^-, E_{th}= 4.4 eV, Table 1) and with the experimental value of (4.5±0.5) eV determined for dissociative excitation of D_3^+ [10]. The cross section displays a broad peak in the region between 5 and 11 eV, centered on 8 eV, with a maximum value of 1.2×10^{-17} cm^2. The presence of this peak is attributed to resonant dissociative excitation (RDE) because it is observed below the threshold for direct dissociative excitation (DDE). Reaction (2) (H^++D+D+e^-, E_{th}= 8.9 eV, Table 1) also contributes to RDE in the H^+ channel and its input is included in the present measurements. For a C_{2v} symmetry structure, the $^2A^1$ excited electronic state of H_3 (dissociation limit: $H_2(X^1\Sigma_g^+)$+H(n=2)) crosses the X^1A^1 fundamental electronic state of H_3^+ (dissociation limit: $H_2(X^1\Sigma_g^+)$+H^+) at H_2–H bond distance of 2.6 a_0 [16]. In the Franck-Condon region, the $^2A^1$ potential energy surface of the excited H_3 neutral lays about 6 eV above that of the ground state of the H_3^+ ion (X^1A^1, v= 0) [16]. The low experimental threshold for H^+ formation can be attributed to an initial capture of the electron into this excited state of H_3 which autoionizes resulting in the dissociation into H_2+H^+ fragments. In addition to the vibrational population and to the resonant capture leading to the low RDE threshold, the large width of the Franck-Condon region associated with the excited vibrational levels must also be taken into account.

The cross section exhibits a second threshold at (11.0±1.0) eV, which is pointed out by the change of slope at this energy. This result is observed to be below the vertical excitation energy calculated for the dissociative excitation of H_3^+ via the first excited triplet state $1^3E'$ at 14.75 eV [13]. The signal measured for energies higher than this second threshold is attributed to non-resonant dissociative excitation. Excitation might also occur from excited

vibrational levels populated within the X^1A_1' ground state that would contribute to enlarge the Franck-Condon region and to lower the thresholds.

Table 2

3.2. D^+ channel

Figure 2(b) shows results for the formation of the D^+ fragment together with the DE contribution (D^++HD, or D^++D+H). As for H^+, unfavorable signal-to-noise ratio prevented us from measuring directly the DI contribution for the D^+ channel so the DI contribution attributed to D^+ is actually that of HD^+ ($HD^+ + D^+ + 2e^-$, reaction (7)). The DI contribution is almost as broad as that of DE and the maximum DI cross section is found to be $(2.03\pm0.04)\times10^{-17}$ cm^2 at 75 eV. The DE contribution (reaction (3) or (4)), which is measured to be larger than that of DI over the whole energy range, is especially broad by comparison to the DE contributions measured for the three other fragments. It exhibits a plateau between 30 eV and 95 eV and its maximum cross section is measured to be $(2.59\pm0.10)\times10^{-17}$ cm^2 at 75 eV.

The D^+ appearance energy threshold that is measured to be (10.5±0.5) eV almost coincides with the direct DE threshold for H^+ (11 eV), but it is 5 eV above the corresponding RDE threshold for (5.5 eV). It indicates that, for D_2H^+, no RDE contribution is detected in the D^+ channel, unlike what is observed for H^+ (within the experimental uncertainties). In the dissociation of D_3^+ leading to the D^+ product, a RDE contribution is apparent in the 4 to 12 eV energy region [10]. There is a strong isotope effect in the dissociation of D_2H^+ favoring the H^+ channel over the D^+ channel in the low energy range below 10 eV. Firstly, the DE process yielding the F^+ fragment may occur via the capture of the incident electron into a T** doubly excited autoionizing dissociative state (resonant dissociative excitation, RDE):

$$e^- + T^+ \rightarrow T^{**} \rightarrow F^+ + \text{neutrals} + e^- \qquad \text{(RDE)}$$

where the T** state is located just above the corresponding dissociation limit. F stands for fragment (H^+, H_2^+ and isotopologues) and T stands for target (H_3^+ and isotopologues). Secondly, the DE process may occur via a direct transition to a $T^{+}*^{(d)}$ dissociative excited state of the target (direct dissociation, DDE). Lastly, the DE process may also occur via a transition to a $T^{+}*^{(b)}$ bound metastable excited state that is coupled with a $T^{+}*^{(d)}$ dissociative excited state (predissociation, PDE):

$$e^- + T^+ \rightarrow T^{+}*^{(b)} + e^- \rightarrow T^{+}*^{(d)} + e^- \rightarrow F^+ + \text{neutrals} + e^- \qquad \text{(PDE)}$$

The peak observed below 10 eV for H^+ is the signature of resonant dissociative excitation. As for predissociation, there is no evidence of its role in the present experiment, above 10 eV. The D^+ appearance energy (10.5 eV) is observed to be lower than the direct DE threshold ($1^3E'$, 14.75 eV) but the shoulder that is merely discernible around (15±1) eV is expected to correspond to the energy threshold of the DE process. A plausible assumption for the observed energy threshold is that excitation occurs from excited vibrational levels populated within the ground state.

3.3. HD^+ channel

Figure 2(c) shows results for the formation of the HD^+ fragment together with the DE contribution (HD^++D). Experimental conditions were favorable enough to allow DE and DI contributions to be obtained separately for HD^+ [14]. Figure 2(e) shows results for the corresponding dissociative ionization contribution (HD^++D^+, reaction (7)). The HD^+ appearance energy threshold is measured to be (8.5±0.5) eV, which is higher than the expected one (H_2^++H+e^-, E_{th}= 6.2 eV). The DE contribution (reaction (5)) is measured to be noticeably higher than that of DI below 40 eV. The shape of the DE cross section is very sharp and its maximum is measured to be (3.12±0.20)×10^{-17} cm^2 at 14 eV.

The dissociative ionization threshold is observed around (15.0±1.0) eV and the maximum cross section is found to be (2.03±0.04)×10^{-17} cm^2 at 75 eV. Such energy is too low to be consistent with a threshold for a direct transition in the Franck-Condon (FC) region corresponding to a DI process and it is also too low to be attributed to the $H^+ + H_2^+ + 2e^-$ reaction (E_{th}= 19.8 eV, Table 1). A distinctive shoulder is discernible at (35.0±1.0) eV, which is expected to correspond to the energy threshold of the DI process. From a full configuration interaction calculation, Gorfinkiel and Tennyson [20] determined the vertical ionization threshold of H_3^+ to be 33.47 eV.

3.4. D_2^+ channel

Figure 2(d) shows results for the formation of the D_2^+ fragment together with the DE contribution (D_2^++H, reaction (6)) and the DI contribution ($H^+ + D_2^+$, reaction (8)) is presented in figure 2(e). As observed for HD^+, the maximum of the cross section is reached for low electron energy, below 20 eV, and the DE contribution is measured to be higher than that of DI below 40 eV. The D_2^+ appearance energy threshold (8.5±0.5 eV) is the same as that of

HD^+ formation and the shape of the DE cross section is sharp as well, its maximum is measured to be $(2.99\pm0.10)\times10^{-17}$ cm^2 at 18 eV.

The threshold energy for the dissociative ionization process is observed to be (18.0±1.0) eV which is reasonably close to the predicted value ($H^+ + H_2^+ + 2e^-$, E_{th}= 19.8 eV). The DI maximum cross section is found to be $(2.03\pm0.04)\times10^{-17}$ cm^2 at 75 eV. As it is the case for the HD^+ fragment, the DI threshold energy is inconsistent with the threshold for a direct transition in the Franck-Condon region (33.47 eV). Nevertheless, a distinctive shoulder is also observed at (35.0±1.0) eV, corresponding to the energy threshold of the direct DI process.

Figure 2

3.5. Isotope effects within D_2H^+

Deuterated molecules undergo chemical fragmentation that may enhance the relative abundance of isotopic fragments. The breakup dynamics and the isotope effects following dissociation of D_2H^+ have been studied by analyzing the isotope ratios $2[H^+ + D_2]/[D^+ + HD]$, $2[D_2^+ + H]/[HD^+ + D]$ and $2[D_2^+ + H^+]/[HD^+ + D^+]$ (Figure 2(f)). To study the isotope ratios within D_2H^+, we consider two-body dissociations only, for clarity reasons.

For DE yielding atomic ions, the ratio $2[H^+ + D_2]/[D^+ + HD]$ is measured to be (0.9±0.1) on average in the 30–1000 eV range. On a purely statistical ground, the D^+ channel should be twice as strong as the H^+ channel so the ratio $2[H^+ + D_2]/[D^+ + HD]$ should be equal to 1. Present result indicates that there is no clear isotope effect above 30 eV. Carrington et al [17] studied the photodissociation of excited D_2H^+ by recording H^+ and D^+ fragment separately. They observed that predissociation results in the formation of H^+ rather than D^+ because the ratio of corresponding signals was equal to three. This result was later corroborated by the theoretical predictions of Pollak and Schlier [18]. Conversely, Badenhoop et al [19] demonstrated that the D_2H^+ ions formed from D_2^+ (v= 18, 24)+H_2 tend to dissociate in favor of the D^+ channel. They also demonstrated that the centrifugal barrier for $D_2H^+ \rightarrow D^+ + HD$ would always be lower than that for $D_2H^+ \rightarrow H^+ + D_2$, resulting in the dissociation favoring D^+ fragments. Present results do not support any of these predictions because the ratio of the cross sections $2[H^+ + D_2]/[D^+ + HD]$ is really close to 1, so that no channel is promoted.

For DE yielding diatomic ions, the D_2^+ channel is clearly favored over the HD^+ one, underlining another unambiguous isotope effect. The ratio of the cross sections $2[D_2^+$

+H]/[HD^++D] is measured to be (2.8±0.4) on average in the 30–1000 eV range. The isotope ratio of the DI cross sections 2[D_2^++H^+]/[HD^++D^+] is observed to be almost constant in the 50–2500 eV, it is measured to be (2.1±0.1) on average. It underlines that an isotope effect takes place above 50 eV, favoring the D_2^+ channel over the HD^+ channel. Statistically the HD^++D^+ channel is 2 times more favorable than the D_2^++H^+ channel. Therefore, if there were no isotope effect, the ratio 2[D_2^++H^+]/[HD^++D^+] would be equal to 1.

To review the study of the isotope effect in the dissociation of D_2H^+ in the 50–2500 eV range: the strongest isotope effect is observed for the dissociative excitation into the heavy ions (2[D_2^++H]/[HD^++D], about 3), followed by dissociative ionization (2[D_2^+ +H^+]/[HD^++D^+], about 2) and finally no isotope effect is observed for dissociative excitation into the light ions (2[H^++D_2]/[D^++HD], about 1). In the low energy range (below 10 eV), a strong resonant process is observed for the H^+ channel only, indicating for a strong isotope effect favoring the H^+ channel over D^+ via RDE (see section 3.2).

For H_3^+, Talbi and Saxon [21] have performed calculations on the ***C_{2v}*** geometries (isosceles triangle) as well as on the ***D_{3h}*** geometries (equilateral triangle). The electronic ground $X\,^1A_1^{'}$ state is bound by 4.6 eV with respect to $H_2(X^1\Sigma^+)$+H^+ (two-body asymptote) and by 9.3 eV with respect to H(1s)+H(1s)+H^+ (three-body asymptote). The first excited state $1^1E'$ in ***D_{3h}*** geometry is degenerate and it splits in $2^1A'$ and $3^1A'$ in ***C_{2v}*** geometry. The potential energy curve corresponding to the $2^1A'$ state is very steep in the Franck-Condon region, it is the lowest one leading to H_2^+ with the dissociation limit $H_2^+(X\,^2\Sigma_g^+)$+H(2s). On the contrary, the curve associated to the $3^1A'$ state is almost flat and it corresponds to H^+ formation (H_2^*+H^+ dissociation limit). Dissociation pathways are such that the potential energy decreases and approaches the minimum value associated with the dissociation limit, following the principle of minimum energy. The large steepness of the $2^1A'$ state may explain for the relative importance of the (D_2^++H) channel and for the concomitant ejection of the lightest H fragment (reaction (6) dominating over reaction (5)). Considering the lightest fragment should be promoted, the (H^++D_2) channel (1) should take over the (D^++HD) channel (3) but the present isotope ratio is close to unity. It appears from theoretical studies that a large majority of the channels, both in ***D_{3h}*** and ***C_{2v}*** geometries, yields H^+ in a way or another, so it becomes difficult to assert which electronic state is more likely to take part in the dissociation process. Nevertheless, the fact that the $3^1A'$ state is almost flat is coherent with

the present observation. As for the ionization process, the corresponding potential energy curves are steep due to the Coulomb effect, so the ejection of the lightest fragment is promoted and ($D_2^+ + H^+$, reaction (8)) dominates over ($HD^+ + D^+$, reaction (7)), in agreement with the present observation.

This argument is supported by the classical potential scattering description [22]: the trajectory of a particle (mass m) in the field of a central potential $U(r)$ is confined to a plane and the total energy of the effective motion is a constant:

$$E = \frac{1}{2} m \left(\frac{dr}{dt} \right)^2 + U(r) + \frac{L^2}{2mr^2} \tag{15}$$

where r is the position of the particle, L is the angular momentum and the term $L^2/2mr^2$ corresponds to the centrifugal potential barrier. Equation (15) can be solved for

$$\frac{dr}{dt} = \left[\frac{2}{m} \left(E - U(r) + \frac{L^2}{2mr^2} \right) \right]^{1/2} \tag{16}$$

This can be inverted and integrated over r, to give the time length t of the motion:

$$t = \sqrt{\frac{m}{2}} \int \frac{dr}{\sqrt{E - U(r) + L^2/2mr^2}} \tag{17}$$

The motion is restricted to the allowed region determined by the range over which the argument of the square root is positive. For two isotopes particles (masses m_1 and m_2) performing the same path in the field of a given potential, it comes finally

$$\frac{t_2}{t_1} = \sqrt{\frac{m_2}{m_1}} \tag{18}$$

This purely classical reasoning indicates that, among isotopic species in the same kinematical conditions (potential and trajectory), the ejection of the lightest particle should be favored. This tendency is confirmed for RDE (H^+ over D^+); for the DE diatomic ions D_2^+ and HD^+, associated with ejection of H and D, respectively and for DI; but not for H^+ and D^+ produced via DE.

Figure 3

3.6. D_2H^+ versus D_3^+ fragmentation

Total (DE+DI) absolute cross sections for electron-impact fragmentation of D_2H^+ are compared with those obtained for the D_3^+ target [10], for the atomic and for the diatomic ions in figures 3(a) and 3(b), respectively. The total cross section for the atomic ions

$(H^+ + D^+)/D_2H^+$ is the sum of the total cross sections for H^+ or D^+ formation and its maximum is measured to be $(7.8\pm0.2)\times10^{-17}$ cm^2 at 75 eV. It is almost a factor of two lower than the maximum cross section obtained for D^+/D_3^+, $(13.9\pm1.1)\times10^{-17}$ cm^2 at 55 eV. Similarly to what is observed for DE (see below), it is clearly apparent that total cross sections for D_2H^+ are found to be lower than those for D_3^+, over the whole energy range. For the diatomic ions, the cross section for $(HD^+ + D_2^+)/D_2H^+$ is the sum of the total cross sections for HD^+ or D_2^+ formation. Cross sections are observed to be lower by 20% than those for D_2^+/D_3^+, between 20 eV to 100 eV, even so both sets of data agree well together in shape. In figure 3(c), for each target independently, we present the ratios of the total cross section for the light ions over those for the heavy ions. First, for the D_3^+ target, the cross section ratio $[D^+]/[D_2^+]$ is measured to be 1.9±0.2. Then, for the D_2H^+ target, the cross section ratio $[H^+ + D^+]/[HD^+ + D_2^+]$ is found to be 1.25±0.04. Both ratios are higher than unity, which indicates that the production of light ions is dominant, whatever the target may be. This effect is even more pronounced for the D_3^+ target than for the D_2H^+ one.

Results for electron-impact dissociation of D_2H^+ are compared with those for the D_3^+ target [10], for DE and DI separately. The DE contributions to atomic ions and to diatomic ions production are compared in figure 4(a) and 4(b), respectively. For DI, the cross sections for D_3^+ are compared with those for D_2H^+ in figure 4(c). The corresponding cross section ratios $\left[X^+/D_3^+\right]/\left[Y^+/D_2H^+\right]$ are presented in figure 4(d) in order to examine the behavior of the two isotopologues. X^+ stands for the production of D^+ or D_2^+ (for the D_3^+ target), while Y^+ stands for the production of $(H^+ + D^+)$ or $(HD^+ + D_2^+)$ (for the D_2H^+ target). The following cross section ratios have been estimated: $[D^+]/[H^+ + D^+]$ (DE for atomic ions), $[D_2^+]/[HD^+ + D_2^+]$ (DE for diatomic ions) and $[D_2^+]/[HD^+ + D_2^+]$ (DI).

The DE cross section for the atomic ions $(H^+ + D^+)/D_2H^+$ is the sum of the DE cross sections for H^+ or D^+ formation, its maximum is found to be $(4.3\pm0.2)\times10^{-17}$ cm^2 at 35 eV. It is a factor of two lower than what is obtained for D^+/D_3^+, $(9.4\pm0.9)\times10^{-17}$ cm^2 at 55 eV. The cross sections for D_2H^+ are found to be lower than those for D_3^+ over the whole energy range. For D_2H^+, the resonant contribution is noticeable below 10 eV, but much less pronounced than in the D_3^+ case because there is no RDE contribution in the D^+ formation from electron-impact dissociation of D_2H^+. In the 30–2500 eV energy range, the ratio of the cross sections

for the atomic ions $[D^+]/[H^+ + D^+]$ is seen to exhibit the less regular behavior of all the calculated ratios. It is estimated to be (2.7±0.4) on average. Irregularities affecting this ratio may be explained by the D^+/D_3^+ cross sections that are affected by larger uncertainties than those for $(H^+ + D^+)/D_2H^+$. The DE cross section for the diatomic ions $(HD^+ + D_2^+)/D_2H^+$ is the sum of the DE cross sections for HD^+ or D_2^+ formation. The $(HD^+ + D_2^+)/D_2H^+$ maximum cross section, $(5.9\pm0.2)\times10^{-17}$ cm^2 at 16 eV, is in reasonable agreement with the maximum cross section for D_2^+/D_3^+, $(6.3\pm0.5)\times10^{-17}$ cm^2 at 18 eV, which is in opposition to what is observed for the atomic ions. Above the maximum, i.e. above 20 eV, the cross sections for D_2H^+ are observed to be lower than those for D_3^+. The ratio of the cross sections for the diatomic ions $[D_2^+]/[HD^+ + D_2^+]$ is observed to be almost constant in the 15–2500 eV range and it is found to be around (1.4±0.2) on average. The DI cross section for D_2H^+ is the sum of the DI cross sections for HD^+ or D_2^+ formation. Overall, the DI cross section for D_2H^+ agrees very well with what is measured for D_3^+. The corresponding maxima are $(4.16\pm0.05)\times10^{-17}$ cm^2 and $(4.3\pm0.2)\times10^{-17}$ cm^2 at 75 eV, for D_2H^+ and D_3^+, respectively. The ratio of the DI cross sections is found to be close to 1 over the whole energy range, it is measured to be (1.07±0.05) on average.

To summarize the comparison between the D_3^+ and D_2H^+ targets, the strongest isotope effect is observed for the dissociative excitation into the light ions ($[D^+]/[H^+ + D^+]$, 2.7), followed by dissociative excitation into the heavy ions ($[D_2^+]/[HD^+ + D_2^+]$, 1.4) and finally no effect is observed for dissociative ionization (isotope ratio close to 1).

The electronic potential energy curves are supposed to be identical for the D_3^+ and D_2H^+ targets under the Born–Oppenheimer approximation and neglecting relativistic effects. But the vibrational and rotational manifolds are supposed to be different for each isotopologues, which corresponds to isotope effects. In the case of D_2H^+, the symmetry is broken because of the mass difference of the H and D nuclei. It causes the center of mass to shift away from the center of charge, creating a dipole moment, which is absent in the homonuclear molecules. Present sets of cross sections allow the quantification of the non-negligible isotope effects for D_2H^+ and D_3^+ which have to be related to these theoretical statements.

Figure 4

4. Conclusion

Absolute cross sections for electron-impact dissociation of D_2H^+ into H^+, D^+, HD^+ and D_2^+ fragments have been measured in the energy region from their respective thresholds to 2.5 keV in the crossed electron–ion beams experiment. The present results for D_2H^+ are compared with those measured for D_3^+ [10]. The analysis of the results brings into evidence significant isotope effects, which are supported by a purely classical reasoning. This reasoning indicates that, among isotopic species in identical kinematical conditions, the ejection of the lightest particle is favored. This tendency is first confirmed for the RDE process, which is observed in the low energy range (5–11eV) for H^+/D_2H^+ only and not for any of the other fragments. Moreover, its contribution is found to be much smaller than the D^+/D_3^+, observed in the previous experiment [10]. For DE, the tendency is confirmed for the molecular products D_2^+ and HD^+, associated with ejection of H and D, respectively, but not for H^+ and D^+ which are found to be of the same importance. Finally, the ejection of the lightest particle is also evident for DI. Present DE cross sections for D_2H^+ are found to be significantly lower than those measured for D_3^+, although those for DI agree well together. Molecular dynamics treatments of these reactions should enlighten the present experimental results.

Acknowledgements

J. Lecointre acknowledges financial support provided by F.R.S.–FNRS (Belgium). X. Urbain is a Senior Research Associate of the F.R.S.–FNRS (Belgium). J. J. Jureta expresses his gratitude for the partial support of the project 141011 from the Ministry for Science and Technology of the Republic of Serbia. This work was supported by the Association Euratom-Belgian State. We thank the Forschungszentrum Jülich for the lending of the ECR ion source and all the staff members of the IMCN for their assistance in this experiment.

References

[1] Geballe TR, McCall BJ, Hinkle KH and Oka T 1999 *Astrophys. J.* **510** 251

[2] Larsson M, Danared H, Mowat JR, Sigray P, Sundström G, Broström L, Filevich A, Källberg A, Mannervik S, Rensfelt KG and Datz S 1993 *Phys. Rev. Lett.* **70** 430

[3] Neufeld DA, Green JD, Hollenbach DJ, Sonnentrucker P, Melnick GJ, Bergin EA, Snell R L, Forrest WJ, Watson DM and Kaufman MJ 2006 *Astrophys. J.* **647** L33

[4] Roueff E and Gerin M 2003 *Space Sci. Rev.* **106** 61

[5] Vastel C, Phillips TG and Yoshida H 2004 *Astrophys. J.* **606** L127
[6] Strasser D, Lammich L, Kreckel H, Krohn S, Lange M, Naaman A, Schwalm D, Wolf A and Zajfman D 2002 *Phys. Rev. A* **66** 032719
[7] Strasser D, Lammich L, Kreckel H, Lange M, Krohn S, Schwalm D, Wolf A and Zajfman D 2004 *Phys. Rev. A* **69** 064702
[8] Datz S, Larsson M, Stromholm C, Sundstrom G, Zengin V, Danared H, Kallberg A, and af Ugglas M 1995 *Phys. Rev. A* **52** 2901
[9] Buhr H, Mendes M B, Novotny O, Schwalm D, Berg MH, Bing D, Heber O, Krantz C, Orlov DA, Rappaport ML, Sorg T, Stutzel J, Varju J, Wolf A and Zajfman D 2010 *Phys. Rev. A* **81** 062702
[10] Lecointre J, Abdellahi El Ghazaly MO, Jureta JJ, Belic DS, Urbain X and Defrance P 2009 *J. Phys. B: At. Mol. Opt. Phys.* **42** 075201
[11] Jensen MJ, Pedersen HB, Safvan CP, Seiersen K, Urbain X and Andersen LH 2001 *Phys. Rev A* **63** 052701
[12] Le Padellec A, Larsson M, Danared H, Larson A, Peterson JR, Rosén S, Semaniak J and Strömholm C 1998 *Phys. Scripta* **57** 215
[13] Faure A and Tennyson J, 2002 *J. Phys. B: At. Mol. Opt. Phys.* **35** 1865
[14] Lecointre J, Belic DS, Cherkani-Hassani H, Jureta JJ and Defrance P 2006 *J. Phys. B: At. Mol. Opt. Phys.* **39** 3275
[15] Defrance P, Brouillard F, Claeys W and Van Wassenhove G 1981 *J. Phys. B: At. Mol. Opt. Phys.* **14** 103
[16] McCall BJ, Huneycutt AJ, Saykally RJ, Djuric N, Dunn GH, Semaniak J, Novotny O, Al-Khalili A, Ehlerding A, Hellberg F, Kalhori S, Neau A, Thomas R, Paal A, Osterdahl F and Larsson M 2004 *Phys. Rev. A* **70** 052716
[17] Carrington A, McNab I R and West Y D 1993 *J. Chem. Phys.* **98** 1073
[18] Pollak E and Schlier C 1989 *Acc Chem. Res.* **22** 223
[19] Badenhoop J K, George C and Eaker C W 1987 *J. Chem. Phys.* **87** 5317
[20] Gorfinkiel JD and Tennyson J 2005 *J. Phys. B: At. Mol. Opt. Phys.* **38** 1607
[21] Talbi D and Saxon RP 1988 *J. Chem. Phys.* **89** 2235
[22] Bransden BH and Joachain CJ 2003 *Physics of Atoms and Molecules* (2nd Edition, Pearson Education, Benjamin Cummings) ISBN: 978-0582356924
[23] NIST Chemistry WebBook, *http://webbook.nist.gov/chemistry/*

Figures and captions

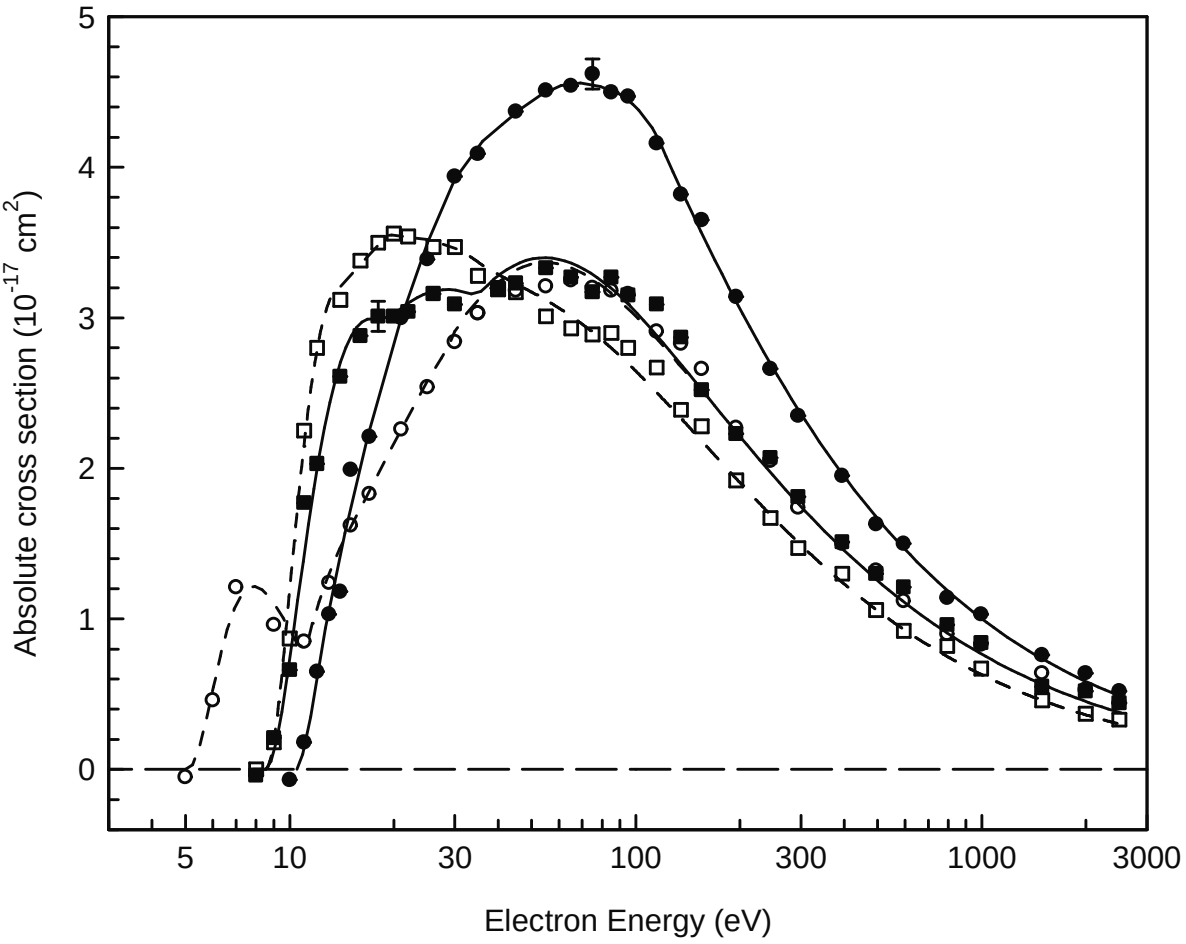

Figure 1. Absolute total cross sections for the fragmentation of D_2H^+ leading to the production of H^+ (○), D^+ (●), HD^+ (□) and D_2^+ (■) versus the electron energy. For clarity reasons, error bar are not presented in the figure. Solid and dashed lines are included to guide the eye.

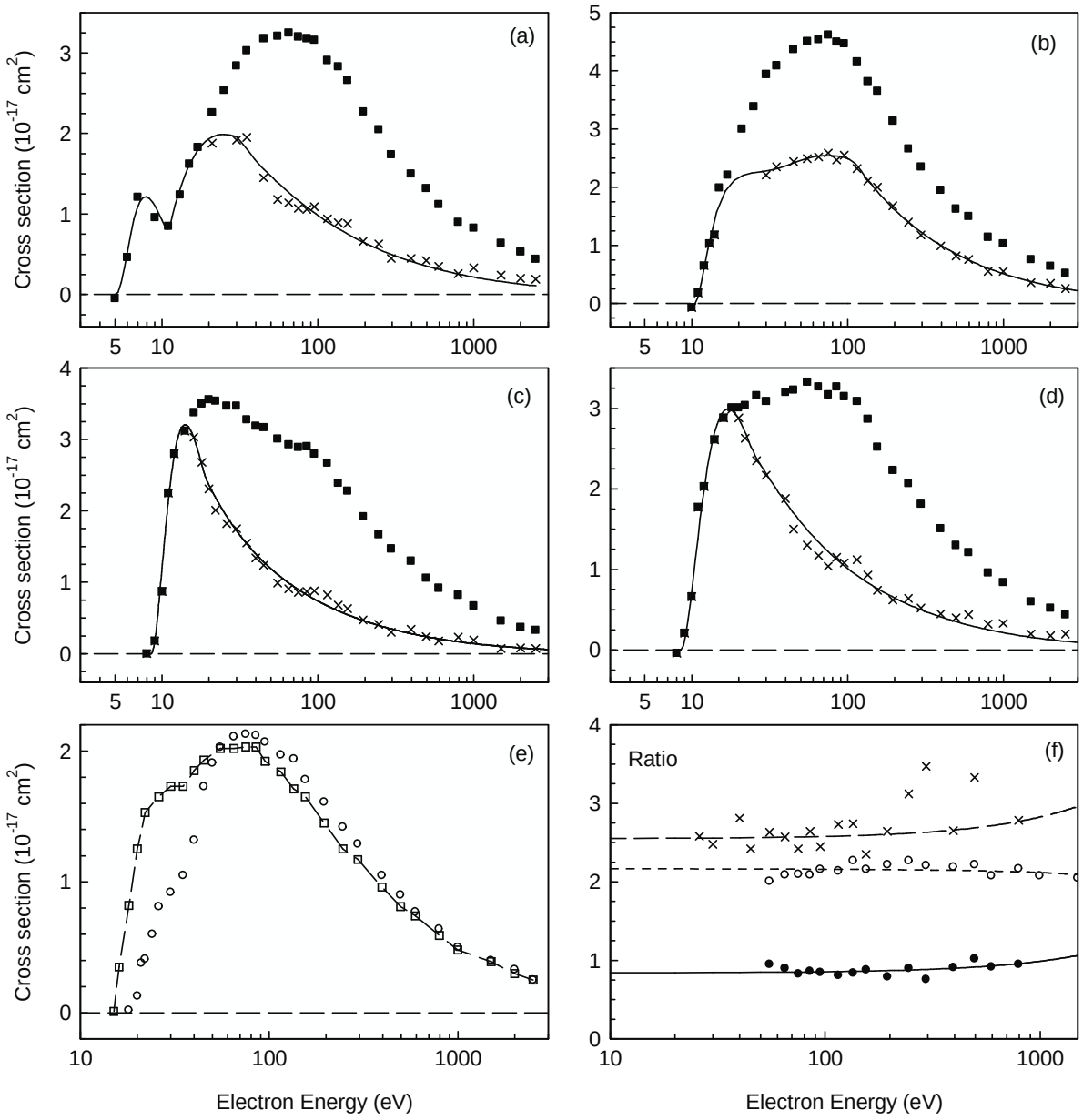

Figure 2. Absolute cross sections (■) for the fragmentation of D_2H^+ leading to the production of (a) H^+, (b) D^+, (c) DH^+ and (d) D_2^+ versus the electron energy, together with the dissociative excitation (DE, ×) contributions. The solid lines are a guide to the eye to help visualize DE contributions. The dissociative ionization (DI) is presented on panel (e) for the channel HD^++D^+ (□) and for the channel D_2^++H^+ (○). Cross section ratios for the dissociative contributions are presented in panel (f): 2[H^++D_2]/[D^++HD] (DE, ●), 2[D_2^++H]/[HD^++D] (DE, ×) and 2[D_2^++H^+]/[HD^++D^+] (DI, ○). See text for details.

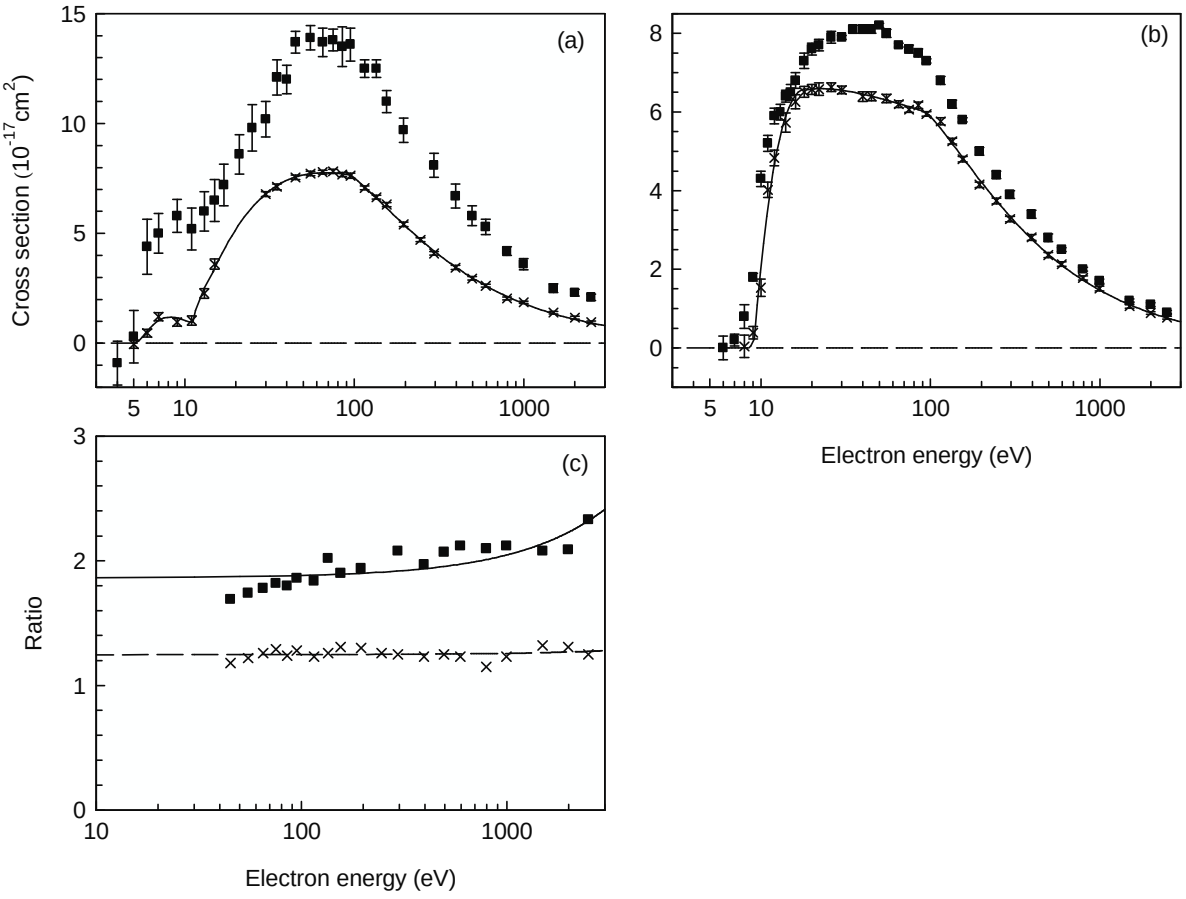

Figure 3. Absolute total cross sections (DE+DI) versus the electron energy

(a) for D^+/D_3^+ (■) and for $\left(H^+ + D^+\right)/D_2H^+$ (×),

(b) for D_2^+/D_3^+ (■) and for $\left(HD^+ + D_2^+\right)/D_2H^+$ (×).

The solid line is a guide to the eye.

(c) Cross section ratio for (■) the D_3^+ target $[D^+]/[D_2^+]$ and for (×) the D_2H^+ target $[H^+ + D^+]/[HD^+ + D_2^+]$. See text for details.

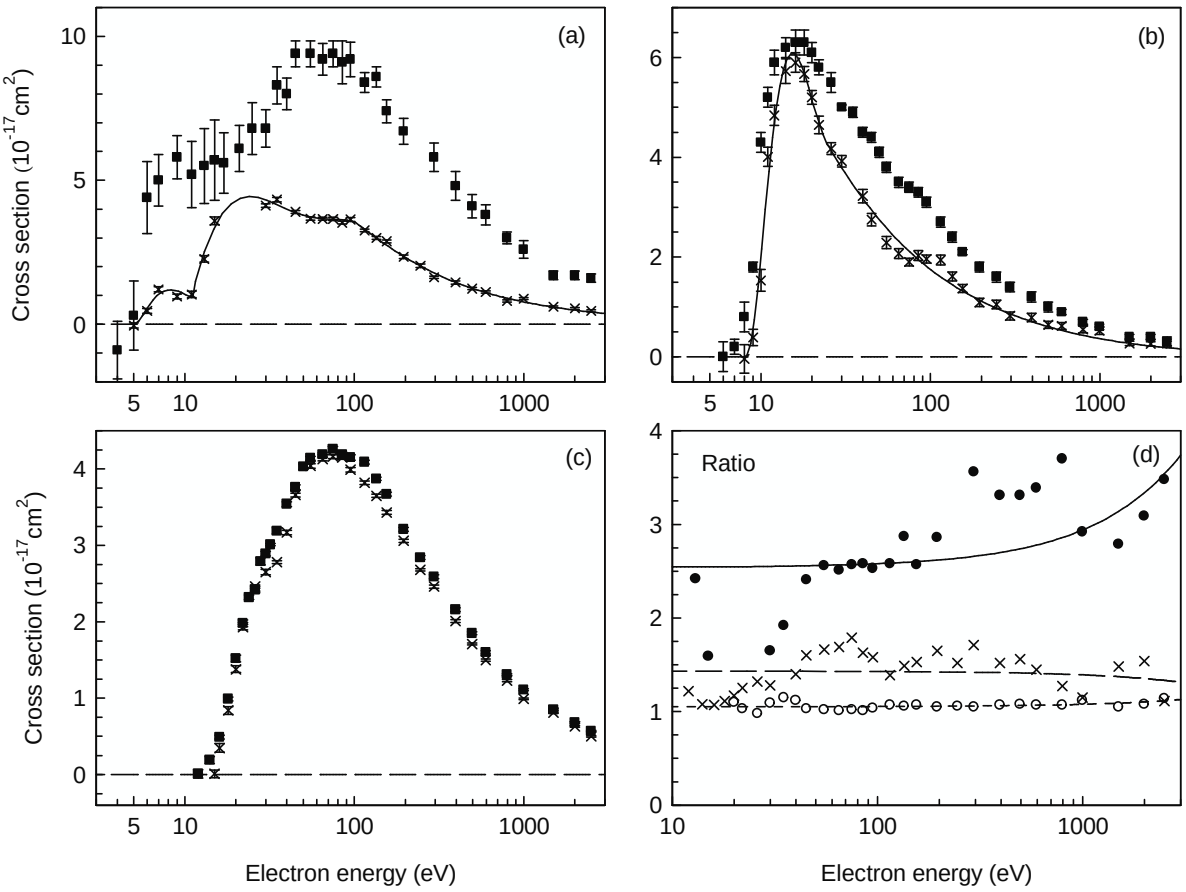

Figure 4. Absolute cross sections versus the electron energy for

(a) DE for D^+/D_3^+ (■) and for $\left(H^+ + D^+\right)/D_2H^+$ (×),

(b) DE for D_2^+/D_3^+ (■) and for $\left(HD^+ + D_2^+\right)/D_2H^+$ (×),

(c) DI for D_2^+/D_3^+ (■) and for $\left(HD^+ + D_2^+\right)/D_2H^+$ (×).

The solid line is a guide to the eye to help visualize DE contribution.

(d) Cross section ratio $\left[X^+/D_3^+\right]/\left[Y^+/D_2H^+\right]$ for the dissociative contributions: $[D^+]/[H^+ + D^+]$ (DE, ●), $[D_2^+]/[HD^+ + D_2^+]$ (DE, ×) and $[D_2^+]/[HD^+ + D_2^+]$ (DI, ○). See text for details.

Dissociation process	H_3^+	Experimental (eV) [1]	Predicted (eV) [2]	D_2H^+	Experimental (eV)
RDE	$H^+ + H_2$	4.5 ± 0.5	4.4	$H^+ + D_2$	5.5 ± 0.5
				$D^+ + HD$	No
RIP	$H^+ + H + H^-$		8.1		
DE	$H^+ + H + H$		8.9	$H^+ + D + D$	11 ± 1
				$D^+ + H + D$	10.5 ± 0.5
		14 ± 1	14.75 ($1^3E'$) [3]		15 ± 1
RIP	$H_2^+ + H^-$		5.8		
DE	$H_2^+ + H$	6.0 ± 0.5	6.2	$HD^+ + D$	8.5 ± 0.5
				$D_2^+ + H$	8.5 ± 0.5
DI	$H^+ + H_2^+$	11.0 ± 0.5 12.0 ± 0.5	19.8	$H^+ + D_2^+$	18 ± 1 (D_2^+)
				$H^+ + D^+ + D$	
DI				$D^+ + HD^+$	15 ± 1 (HD^+)
	$H^+ + H^+ + H$		22.5	$D^+ + H^+ + D$	
			33.47 (FC) [4]		35 ± 1 (HD^+) 35 ± 1 (D_2^+)

Table 1. Threshold energies (eV) for the dissociation of H_3^+ and of D_2H^+.

[1] [10] (D_3^+ target), [2] [23], [3] [13], [4] [20]

Note: RIP (Resonant-Ion-Pair formation) and FC (Franck-Condon)

Table 2: Absolute total cross sections (H^+, D^+, HD^+ and D_2^+, 10^{-17} cm^2).

	H^+		D^+		HD^+		D_2^+	
E (eV)	σ	Δσ	σ	Δσ	σ	Δσ	σ	Δσ
5	-0.05	0.18						
6	0.46	0.17						
7	1.21	0.18						
8					0.00	0.30	-0.04	0.27
9	0.96	0.17			0.18	0.26	0.21	0.06
10			-0.07	0.11	0.87	0.35	0.66	0.09
11	0.85	0.20	0.18	0.23	2.25	0.17	1.77	0.22
12			0.65	0.17	2.80	0.26	2.03	0.14
13	1.24	0.22	1.03	0.23				
14			1.18	0.24	3.12	0.20	2.61	0.29
15	1.62	0.20	1.99	0.27				
16					3.38	0.18	2.88	0.18
17	1.83	0.13	2.21	0.09				
18					3.50	0.18	3.01	0.10
20					3.56	0.15	3.01	0.10
21	2.26	0.12	3.00	0.16				
22					3.54	0.16	3.04	0.15
25	2.54	0.15	3.39	0.09				
26					3.47	0.12	3.16	0.09
30	2.84	0.11	3.94	0.11	3.47	0.12	3.09	0.08
35	3.03	0.13	4.09	0.15	3.28	0.07		
40					3.19	0.12	3.20	0.12
45	3.18	0.09	4.37	0.10	3.17	0.11	3.23	0.11
55	3.21	0.12	4.51	0.08	3.01	0.10	3.33	0.11
65	3.25	0.08	4.54	0.09	2.93	0.08	3.27	0.09
75	3.20	0.11	4.62	0.09	2.89	0.08	3.17	0.06
85	3.18	0.10	4.50	0.09	2.90	0.09	3.27	0.08
95	3.16	0.06	4.47	0.16	2.80	0.08	3.15	0.04
115	2.91	0.05	3.82	0.09	2.67	0.10	3.09	0.08
135	2.83	0.08	3.65	0.09	2.39	0.07	2.87	0.08
155	2.66	0.09	3.56	0.11	2.28	0.08	2.52	0.06
195	2.27	0.08	3.14	0.12	1.92	0.06	2.23	0.08
245	2.05	0.06	2.66	0.13	1.67	0.08	2.07	0.06
295	1.74	0.07	2.35	0.09	1.47	0.08	1.81	0.06
395	1.50	0.08	1.95	0.10	1.30	0.08	1.51	0.07
495	1.32	0.07	1.63	0.09	1.06	0.07	1.30	0.05
595	1.12	0.05	1.50	0.08	0.92	0.04	1.21	0.07
795	0.90	0.06	1.14	0.08	0.82	0.06	0.96	0.05
995	0.83	0.04	1.03	0.06	0.67	0.06	0.84	0.06
1495	0.64	0.06	0.76	0.05	0.46	0.05	0.55	0.04
1995	0.53	0.06	0.64	0.06	0.37	0.04	0.52	0.03
2495	0.44	0.06	0.52	0.06	0.33	0.03	0.44	0.04